A&A 382, 921–934 (2002)
DOI: 10.1051/0004-6361:20011612

Astronomy & Astrophysics

Radio and submillimetre observations of ϵ Ori

R. Blomme[1], R. K. Prinja[2], M. C. Runacres[1], and S. Colley[2]

[1] Royal Observatory of Belgium, Ringlaan 3, 1180 Brussel, Belgium
[2] Department of Physics & Astronomy, University College London, Gower Street, London WC1E 6BT, UK

Received 16 October 2001 / Accepted 7 November 2001

Abstract. In common with other early-type stars, ϵ Ori (B0 Ia) shows evidence for structure in its stellar wind. Variations in optical and ultraviolet line profiles reveal the presence of *large-scale* structure in the inner wind. The detection of X-rays and the existence of black troughs in saturated ultraviolet lines are indicative of *small-scale* structure. The geometric extent of both types of structure is poorly known. In principle, large-scale structure can be detected directly from very high spatial resolution observations that resolve the stellar wind. A simpler technique is to look for the presence of additional flux compared to that expected from a smooth wind. The run of this excess flux as a function of wavelength indicates how fast structure decays in the wind. If there is variability in the excess flux, it shows us that the structure must be large-scale. Such variability is suggested by two previous 6 cm radio observations of ϵ Ori: Abbott et al. (1980) found 1.6 ± 0.5 mJy, while Scuderi et al. (1998) measured only 0.60 ± 0.06 mJy. This could indicate that the large-scale structure persists beyond $\sim$50 R_*. To further investigate this variability, we used the Very Large Array (VLA) to monitor ϵ Ori over a 5-day period in February 1999. We supplemented our data with observations from the VLA archive. In an attempt to resolve the stellar wind, we also obtained a series of high spatial resolution observations with the Multi-Element Radio Linked Interferometer Network (MERLIN) during January–March 1999. From this combined material we find no evidence for variability and we conclude that the Abbott et al. (1980) flux determination is in error. The data do show substantial excess flux at millimetre wavelengths, compared to a smooth wind. This excess is confirmed by a submillimetre observation which we obtained with the James Clerk Maxwell Telescope (JCMT). The behaviour of ϵ Ori is therefore similar to what had been found previously for α Cam, δ Ori A, κ Ori and ζ Pup. While the present data do not allow very strong constraints, they show that considerable structure must persist up to at least $\sim$10 R_* in the wind of ϵ Ori. The combined radio fluxes are used to derive a mass-loss rate of $\log \dot{M}(M_\odot/\mathrm{yr}) = -5.73 \pm 0.04$. This value is in good agreement with the Hα mass-loss rate. The good agreement between Hα and radio mass-loss rates for hot stars in general remains puzzling, as it implies that the same amount of structure is present in very different formation regions.

Key words. stars: early-type – stars: individual: ϵ Ori – stars: mass-loss – stars: winds, outflows – radio continuum: stars

1. Introduction

Epsilon Ori (HD 37128; B0 Ia) is the middle star in the Belt of Orion. A star of this spectral type has a stellar wind which is driven by radiation pressure. The stellar-wind material emits free-free radiation (bremsstrahlung) that is detectable at radio and millimetre wavelengths. Radio observations are the preferred data for determining the mass-loss rates of early-type stars, as the interpretation of these fluxes is not strongly dependent on details of the wind velocity law or ionization conditions (e.g. Wright & Barlow 1975; Abbott et al. 1980).

Radio and millimetre emission have two further extremely useful characteristics. First, the high bremsstrahlung opacity is proportional to the *wavelength* squared. Therefore, the observed emission originates above a characteristic radius that increases with wavelength (typical values are $\sim$5 R_* at 1 mm and $\sim$100 R_* at 20 cm). Secondly, free-free emission also depends on the *density* squared. This makes it a good indicator of structure. The combination of these two properties means that by comparing emission at increasing wavelengths we can investigate how structure decays as it moves out with the stellar wind.

It is important to distinguish between two kinds of structure. On the one hand there is widespread observational evidence of large-scale, coherent structure, most notably the Discrete Absorption Components (DACs) that move through unsaturated UV spectral lines. Their rotational modulation strongly suggests that the structure is somehow rooted to the surface of the star (see review by Prinja 1998). On the other hand, high X-ray luminosities

Send offprint requests to: R. Blomme,
e-mail: Ronny.Blomme@oma.be

(Sciortino et al. 1990) and especially the broad regions of total absorption ("black troughs") in saturated P Cygni profiles (Lucy 1982) are indicative of small-scale stochastic structure. The existence of either kind of structure of course complicates the mass-loss rate determination from the radio fluxes.

The large-scale structure is believed to be Co-rotating Interaction Regions (CIRs; Mullan 1986), caused by the interaction of fast and slower streaming gas. These CIRs have been hydrodynamically modelled and may explain the recurrent behaviour of the substantial variability in wind-formed spectral lines (Cranmer & Owocki 1996). Small-scale structure is a result of the instability of the line-driving mechanism (e.g. Owocki 2000).

Ideally, one would want a unified picture of how these two kinds of structure coexist in the stellar wind. A first attempt to theoretically provide such a picture has been made by Owocki (1999). On the observational side, a first step is to put geometric constraints on the structure. This is a key aim of the present paper. Measuring fluxes at millimetre and radio wavelengths will show how fast structure decays. Any variability at a given wavelength indicates that the structure in that particular formation region is large-scale. One can also try to detect the large-scale structure directly, by spatially resolving the stellar wind. All these techniques will be attempted in the present paper.

ϵ Ori is one of the very few normal early-B supergiants that have been detected at radio wavelengths. Abbott et al. (1980) used the Very Large Array (VLA) in 1978 to measure a flux of 1.6 ± 0.5 mJy at 6 cm. In 1994, Scuderi et al. (1998) measured the star again and found only 0.60 ± 0.06 mJy at 6 cm, implying that the radio flux is variable.

This variability is suggestive of large-scale structure persisting up to large distances from the star. It is of course risky to base such a conclusion on only two data points. To examine in detail the apparent radio variability of ϵ Ori, we observed it with the NRAO VLA[1] (National Radio Astronomy Observatory Very Large Array) at 3.6 and 6 cm during 5 consecutive days (for 1 hour per day) in 1999. The range of 5 days covers about one third of the estimated rotation period of this star, enough to see if variability is somehow connected to the photosphere. An additional VLA observation was made almost 2 years later. We also attempted to obtain resolved images of ϵ Ori using the Multi-Element Radio Linked Interferometer Network (MERLIN[2]). Similar techniques have already been applied to a number of early-type stars, e.g. the Be star ψ Per (Dougherty & Taylor 1992), the Luminous Blue Variable P Cygni (White & Becker 1982; Skinner et al. 1997) and the Wolf-Rayet component of the binary WR 147 (Williams et al. 1997). We also observed ϵ Ori at 850 μm with the James Clerk Maxwell Telescope (JCMT[3]).

Our VLA and MERLIN observations allow us to look for variability on a time-scale of days and weeks/months. Furthermore, our additional VLA observation and other observations in the VLA archive allow us to cover a time-scale of many years.

Our adopted parameters of ϵ Ori are provided in Sect. 2. In Sect. 3 we present our VLA observations, and discuss the archive data in Sect. 4. Our MERLIN and JCMT observations are presented in Sects. 5 and 6, respectively. The interpretation of the observational material is discussed in Sect. 7 and conclusions are drawn in Sect. 8.

2. The parameters of ϵ Ori

The stellar parameters are listed in Table 1. The star is a MK standard of spectral type B0 Ia. ϵ Ori is listed as a photometrically variable star in the Mermilliod (1987) catalogue of UBV data. The low level of variability (range in V magnitude is 0.05) is confirmed by photometry from Hipparcos (ESA 1997).

Effective temperature, gravity and turbulent velocity are based on either plane-parallel hydrostatic nonlocal thermodynamic equilibrium (NLTE) models (McErlean et al. 1999), or on unified NLTE models (i.e. models that are spherically symmetric and include a stellar wind – Kudritzki et al. 1999). The McErlean et al. model derives the effective temperature, gravity and He abundance from fitting the equivalent widths of a number of hydrogen and helium lines. The Kudritzki et al. model adopts the McErlean et al. value for the effective temperature and determines the gravity and mass-loss rate from fitting the shape of the Balmer lines. The gravity found by Kudritzki et al. ($\log g = 3.00$) is not significantly different from the McErlean et al. value ($\log g = 2.94 \pm 0.1$). While a higher than solar He abundance has been claimed for ϵ Ori, $Y = N_{\rm He}/(N_{\rm H} + N_{\rm He}) = 0.2$ (Kudritzki et al. 1989), taking into account microturbulence leads to a solution where the He abundance is solar, i.e. $Y = 0.1$ (McErlean et al. 1998).

The luminosity is derived from the continuum flux distribution of the models and the distance. The distance measured by Hipparcos (ESA 1997) and the one derived from ϵ Ori's membership of the Ori OB1 association are compatible. The radius can then be derived from the effective temperature and the luminosity. The radius-distance combination can be checked because ϵ Ori is one of the few early-type stars for which an angular diameter has been determined using optical interferometry techniques.

[1] The National Radio Astronomy Observatory is a facility of the National Science Foundation operated under cooperative agreement by Associated Universities, Inc.

[2] MERLIN is a national facility operated by the University of Manchester at the Nuffield Radio Astronomy Laboratories, Jodrell Bank, on behalf of the Particle Physics and Astronomy Research Council (PPARC) in the UK.

[3] The JCMT is operated by the Joint Astronomy Centre in Hilo, Hawaii on behalf of the parent organizations Particle Physics and Astronomy Research Council in the UK, the National Research Council of Canada and The Netherlands Organization for Scientific Research.

Table 1. Stellar parameters of ϵ Ori.

parameter	value	reference
RA (J2000)	$05^{\rm h}36^{\rm m}12^{\rm s}.8135$	SIMBAD
Dec (J2000)	$-01^\circ12'06''.911$	catalogue
V magnitude	1.71	M87
$B-V$	-0.20	M87
$E(B-V)$	0.081	S77
D	412^{+246}_{-113} pc	Hipparcos
	500 pc	H78
association	Ori OB1	H78
spectral type	B0 Ia	JM53
$T_{\rm eff}$	28500 ± 1000	M99, K99
log g	3.00	K99
Y	0.1	M98
$v_{\rm turb}$	20 km s^{-1}	K99
$v \sin i$	80 km s^{-1}	K99
log $L/L_\odot$	5.50 (Hipparcos distance)	M99
	5.86 (H78 distance)	K99
R_*	35 $R_\odot$	K99
v_∞	1 600 km s^{-1}	K99

References:

H78	Humphreys (1978)
JM53	Johnson & Morgan (1953)
K99	Kudritzki et al. (1999)
M87	Mermilliod (1987)
M98	McErlean et al. (1998)
M99	McErlean et al. (1999)
S77	Snow et al. (1977).

The Kudritzki et al. (1999) value for the radius (35 $R_\odot$) combined with the 500 pc distance gives an angular diameter $\theta = 0.65$ milli-arcsec which is in agreement with the 0.69 ± 0.04 milli-arcsec of Hanbury Brown et al. (1974).

Groenewegen & Lamers (1989) determined the terminal velocity of the wind by detailed profile fitting of the ultraviolet resonance lines and found $v_\infty = 1\,500 \pm 150$ km s^{-1}. Prinja et al. (2001) adopt a value of 1 700 km s^{-1}, while Kudritzki et al. (1999) use 1 600 km s^{-1}. The mass-loss determinations, which are mostly based on radio or Hα, will be discussed in Sect. 7.2.

Variability in the wind-formed spectral lines of ϵ Ori is similar to that seen in many other early-type stars. Ebbets (1982) and Levato et al. (1988) showed that the hydrogen lines are variable. Scuderi (1994) found variability in Hα on time-scales of a day or less. Nightly spectra, secured over several months in 1996, and more intensive data acquired over a few weeks in 1998, indicate that there are substantial changes in the Hα profile over a time-scale of days, which points to large-scale structure in the inner-wind region (i.e. below $\sim$3 R_* – Kaufer et al. 2001). Although polarisation was looked for, none intrinsic to the star or stellar wind was found (Lupie & Nordsieck 1987).

The UV resonance lines are highly variable as well, on time-scales down to hours (e.g. Prinja et al. 2001). Prinja & Howarth (1986) and Prinja et al. (1990) find 2 sets of Discrete Absorption Components in N V and Si IV that go up to 1 725 km s^{-1}. Therefore the UV data also highlight that large-scale, coherent, structure is present.

ϵ Ori also emits X-rays (e.g. Berghöfer et al. 1996). The X-ray luminosity is close to the canonical value (Pallavicini et al. 1981) of $\log L_{\rm X}/L_{\rm bol} = -7$. Additional emission was detected at energies >2 keV with the Solid State Spectrometer on board of the Einstein Observatory (Cassinelli & Swank 1983), which Chen & White (1991) interpret as being nonthermal. Cassinelli et al. (1983) and Collura et al. (1989) looked for variability in X-rays with the Imaging Proportional Counter on board the Einstein Observatory, but found none.

Table 2. Archive data and own data for ϵ Ori.

programme name	date	λ (cm)	ref.
Archive data			
VLA			
BIEG	1978-11-05	6	A80
NEWE	1979-08-08	6	
EBC	1981-08-28	6	
AB268	1983-12-18	20	
AA29	1984-04-04	2+6	
AA47	1985-06-12	2+6	
AJ133	1986-03-21	6	
AP173	1989-10-06	20	
—	1989-12-23	20+90	
AH394	1990-01-29	3.6	H00
AH394	1990-01-30	6	H00
AS544	1994-10-12	2+3.6+6	S98
AJ248	1995-06-19	6	
AC308	1996-09-30	20	C98
Own data			
VLA			
AB901	1999-02-05	3.6+6	
AB901	1999-02-06	3.6+6	
AB901	1999-02-07	3.6+6	
AB901	1999-02-08	3.6+6	
AB901	1999-02-09	3.6+6	
AB901	2000-12-21	6	
MERLIN			
MN/99A/7	1999-01-28	6	
	1999-02-25	6	
	1999-03-03	6	
	1999-03-09	6	
JCMT			
M00BU20	2000-10-12	0.0850	

References:
A80: Abbott et al. (1980)
H00: Howarth (2000, personal communication)
S98: Scuderi et al. (1998)
C98: Condon et al. (1998).

3. VLA observations

3.1. Data

Table 2 lists all radio and submillimetre data discussed in this paper.

We collected observations of ϵ Ori during 5 consecutive days (1999 February 5–9) at 3.6 cm (X-band) and 6 cm (C-band). One observation at 6 cm consists of observing the flux calibrator 3C147= 0542 + 498 (J2000) for one minute, followed by 2 series of alternating between the phase calibrator 0522+012 (J2000) (for 2 min) and ϵ Ori (for 8 min). The procedure for 3.6 cm is quite similar, except that we integrate for 8–12 min on ϵ Ori. For the February 7 observation, we only obtained one series of 3.6 cm observations, instead of the standard two. For each wavelength, all observations were made in 2 sidebands (denoted IF1 and IF2), each of which has a bandwidth of 50 MHz.

The configuration of the VLA array was CD, i.e. the antennas in the East and West arm were in the most compact (D) configuration, while those in the North arm were in the less compact C configuration. For the February 5 observations, 2 antennas in the West arm were in C configuration positions.

We also obtained an additional 6 cm observation on 2000 December 21, while the VLA was in the A configuration (i.e. the configuration with the highest spatial resolution). The target was observed twice for 8 min. This observation served mainly to test the effect of various primary calibrators (3C147 and 3C48 = 0137 + 331) and secondary calibrators (0522 + 012, 0607 − 085 and 0541 − 056) on the ϵ Ori flux. The reasons for these tests are explained in Sect. 4.2.

Table 3. Fluxes of the primary calibrators used in the reduction of our own VLA data and the archive data. The fluxes are based on the 1995.2 VLA coefficients (Perley & Taylor 1999). The two values for each entry correspond to the two 50 MHz sidebands (IF1 and IF2).

λ	freq	flux (mJy)		
(cm)	(GHz)	3C48	3C147	3C286
2	14.9149	1.8099		3.4321
	14.9649	1.8036		3.4234
3.6	8.4149	3.2424		5.2001
	8.4351		4.8235	
	8.4649	3.2234		5.1787
	8.4851		4.7971	
6	4.8351	5.5424	8.0118	7.5103
	4.8851	5.4891	7.9387	7.4617
20	1.41125	16.0817		
	1.46125	15.6477		
	1.4649	15.6170		15.6170
	1.5149	15.2078		15.2078
	1.6351	14.3079		
90	0.3275	42.5471		
	0.333	42.1664		

3.2. Reduction

The data reduction was done using the Astronomical Image Processing System (AIPS), developed by the NRAO. The reduction consists of first determining the instrumental gains (which are complex numbers) from the observed visibilities of the calibrators. Discrepant points are flagged and the process is iterated. The final instrumental gains are interpolated in time and applied to the ϵ Ori visibilities. The Fourier transform is then applied to convert these calibrated visibilities into an intensity map (called the dirty map). In this procedure, weights are assigned to the visibilities (for which various possibilities exist – see Sect. 3.3).

The flux-density scale is based on the work by Baars et al. (1977), modified for the VLA (Perley & Taylor 1999). The fluxes assigned to our primary calibrator are given in Table 3.

As the antennas had been moved not long before our 1999 February observation (and even in between our observations), the positions and baselines were at the time not completely well-determined. From observations performed later by the VLA, the baselines could be better determined. This results in a set of baseline corrections which we applied during the reduction.

We also followed the recommendation of the VLA Calibrator Manual (Perley & Taylor 1999) regarding the number of antennas and the range on projected baselines to be used for any given calibrator to ensure that it can be treated as a point source.

The dirty map is then processed further to remove the effect of the beam (point spread function). The images were deconvolved using the CLEAN algorithm as implemented in AIPS (see e.g. Cornwell & Braun 1994). The resulting images are shown in Figs. 1 and 2d. The 1999 February images show not only ϵ Ori, but also a second source at about 1 arcmin distance. This second source is on the limit of being resolved with the configuration used (it is resolved in some of the observations from the VLA archive – see Sect. 4.1).

3.3. Fluxes and error bars

We measure the fluxes on the clean image, using the AIPS task JMFIT to fit elliptical Gaussians to the source. At the spatial resolution obtained, ϵ Ori is still a point source, so the elliptical Gaussian should have the same form as the cleaned beam, i.e. the same major and minor axis and the same position angle. We therefore took these parameters to be known and only varied the total flux in the fitting procedure. The source fluxes so determined agree very well with the maximum values of intensity on the source (to within better than 1 σ, except for the 2000 December 21 observation where the total flux is 1.23 σ larger than the maximum intensity). This shows that the source can be well approximated by an elliptical Gaussian with the shape of the beam.

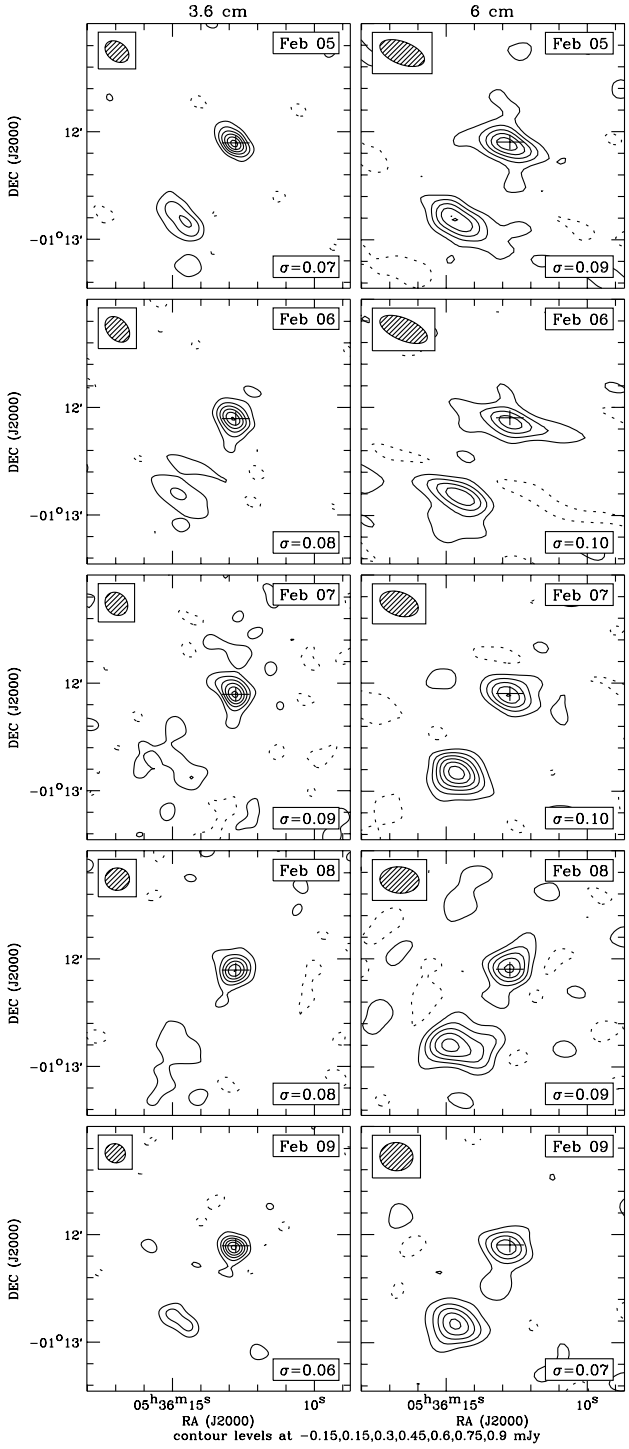

Fig. 1. Maps at 3.6 cm and 6 cm of the 1999 February observations. The beam is given in the upper left corner. The RMS noise in the map is indicated (σ in mJy). The first positive contour line is about 2 σ for the 3.6 cm maps, and about 1.5 σ for the 6 cm maps. The negative contour is indicated by the dashed line. The crosses indicate the optical (Hipparcos) positions. The bars are 1000× larger than the Hipparcos error bars.

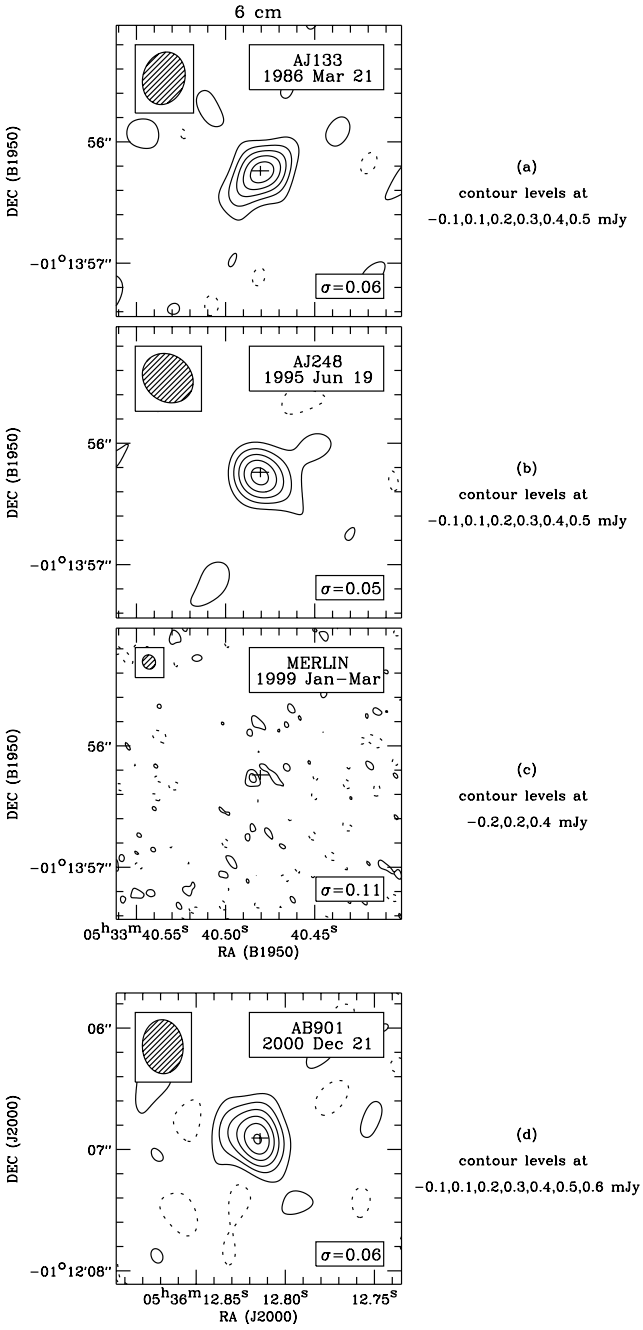

Fig. 2. Maps of the high spatial resolution 6 cm observations. The RMS noise in the map is indicated (σ in mJy). Note the very different spatial scale compared to Fig. 1. The bars indicating the optical (Hipparcos) position are 10× larger than the Hipparcos error bars. Note the good agreement between the radio and Hipparcos positions.

The error determination on the flux (and other quantities) is described in Condon (1997), but the AIPS help files list those errors as tentative. When image data consist of *independent* brightness determinations for a grid of pixels, it is straightforward to determine the error bars on the resulting parameters of a fit. The images from a radio interferometer do not have this independency because they are the result of the Fourier transform of a set of visibilities (which are the independent data), followed by a cleaning operation. It is quite difficult to apply standard error analysis to this type of procedure.

Table 4. ϵ Ori fluxes (in mJy) measured on our own data and the archive data.

progr	date	850 μm	2 cm	3.6 cm	6 cm	20 cm	90 cm	notes
NEWE	1979-08-08				<0.9			
AB268	1983-12-18					<0.57		
AA29	1984-04-04				0.67 ± 0.10			
AA47	1985-06-12		<1.48		<0.7			
AJ133	1986-03-21,22				0.52 ± 0.06			
AP173	1989-10-06					<16		1
—	1989-12-23					<52	<105	1
AH394	1990-01-29			0.92 ± 0.05	0.71 ± 0.06			
AS544	1994-10-12		1.65 ± 0.20	1.00 ± 0.06	0.69 ± 0.06			2
AJ248	1995-05-19				0.47 ± 0.05			
MERLIN	1999-01-28→03-09				0.51 ± 0.11			
AB901	1999-02-05			0.95 ± 0.07	0.94 ± 0.09			
AB901	1999-02-06			0.95 ± 0.08	0.77 ± 0.10			
AB901	1999-02-07			1.01 ± 0.09	0.81 ± 0.10			
AB901	1999-02-08			0.95 ± 0.08	0.78 ± 0.09			
AB901	1999-02-09			0.95 ± 0.06	0.77 ± 0.07			
JCMT	2000-10-12	17.3 ± 2.1						
AB901	2000-12-21				0.70 ± 0.06			3
average		17.3 ± 2.1	1.65 ± 0.20	0.96 ± 0.08	0.74 ± 0.13			4

Notes:
1. Values have been corrected for the effect of the primary beam.
2. AS544 fluxes are based on primary calibrator 3C48. The 2 cm fluxes based on 3C286 are somewhat higher (1.79 ± 0.28 mJy).
3. AB901 2000-12-21 data are with primary 3C147 and secondary $0522 + 012$.
4. Average for 6 cm does not include AJ133 or MERLIN data, for reasons explained in Sects. 4.2 and 5.

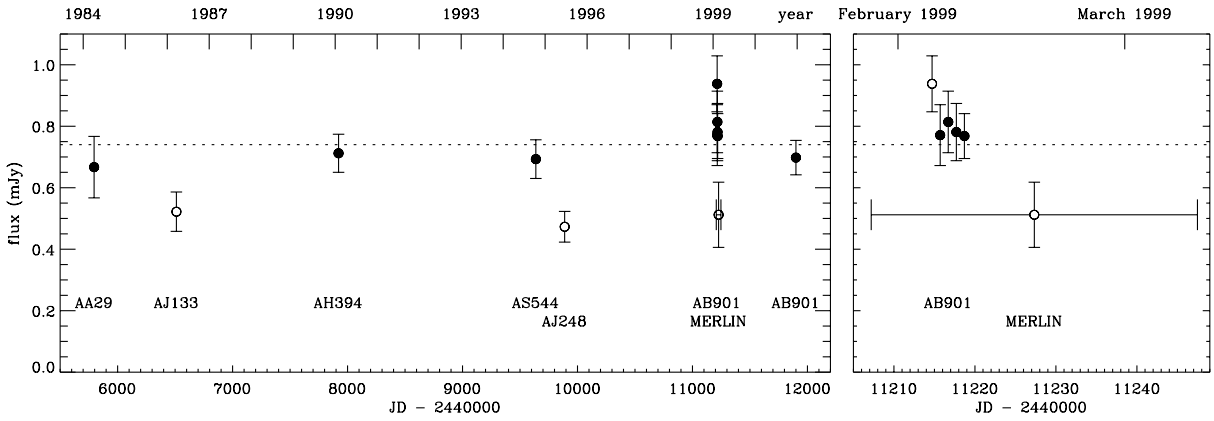

Fig. 3. The 6 cm fluxes of ϵ Ori as a function of time. The panel on the right gives a more detailed view of our 1999 observations. The open circles indicate observations that might show problems (see Sects. 3.3, 4.2 and 5). The average (dotted line) does not include the AJ133 and MERLIN observations, for reasons explained in Sects. 4.2 and 5.

The recommended practice is to use the RMS noise in the total resulting map as an estimate of the error on the flux of a point source (which is the only parameter we want to determine). If the fit parameters give a higher error than the RMS in the map, this higher error should be used (though this never happened in our case). We also checked that the RMS in the total map is not very different from the RMS of the empty upper left quadrant of each map.

In the error analysis we should also include the errors due to the calibration. The VLA Calibrator manual lists 2–3% errors on the calibration. We therefore added (in RMS sense) an error of 0.03 times the observed flux to the other errors.

We did some testing to get a feel for the systematic errors. This was done by varying the various parameters that play a role in the reduction process. In most cases the systematic errors are below the random errors and we therefore consider them to be included in the error bar for the random errors. Care must be taken however with cleaning and weighting. We stop cleaning when the algorithm starts finding about the same number of negative as positive components. For the weighting we use robust uniform weighting (Briggs 1995). While natural weighting

Table 5. Reduction of the VLA archive data. Column (1) gives the programme name, Col. (2) the date of the observation, Col. (3) the wavelength (in cm), Col. (4) the configuration the VLA was in at the time of the observation, Col. (5) the name of the primary calibrator used, Col. (6) the secondary calibrator, Col. (7) the integration time (in minutes) of the target and Col. (8) the beamsize in arcsec^2.

(1) progr.	(2) date	(3) λ	(4) configuration	(5) primary	(6) secondary	(7) int.time	(8) beamsize	notes
BIEG	1978-11-05,06	6		3C286	0529+075	214	—	1
NEWE	1979-08-08	6		3C147	0529+057	102	5.0 × 0.47	
EBC	1981-08-28	6	D	3C286	0500+019	57	13. × 5.8	2
AB268	1983-12-18	20	BnA	3C48	0539−057	10	4.5 × 1.5	
AA29	1984-04-04	6	B=>C	3C286	0539−057	14	10. × 4.6	
AA29	1984-04-04	2	B=>C	3C286	0539−057	14	—	3
AA47	1985-06-12	6	B=>C	3C48	0539−057	16	20. × 2.8	
AA47	1985-06-12	2	B=>C	3C48	0539−057	32	3.5 × 0.49	
AJ133	1986-03-21,22	6	A	3C286	0605−085	48	0.52 × 0.40	
AP173	1989-10-06	20	DnC	3C48	0539−057	5	40. × 19.	
——	1989-12-23	20	D	3C48	0539−057	11	68. × 44.	
——	1989-12-23	90	D	3C48	0518+165	13	223. × 199.	
AH394	1990-01-30	6	D	3C286	0539−057	30	22. × 16.	
AH394	1990-01-29	3.6	D	3C286	0539−057	52	15. × 8.	
AS544	1994-10-12	6	CnB	3C48	0539−057	20	5.5 × 4.5	
AS544	1994-10-12	3.6	CnB	3C48	0539−057	20	2.6 × 2.3	
AS544	1994-10-12	2	CnB	3C48	0539−057	24	2.3 × 1.1	
AJ248	1995-06-19	6	A	3C286	0605−085	85	0.51 × 0.40	
AB901	1999-02-05→09	6	CD	3C147	0522+012	5×16	19. × 14.	
AB901	1999-02-05→09	3.6	CD	3C147	0522+012	5×20	12. × 11.	
AB901	2000-12-21	6	A	various	various	16	0.42 × 0.39	

Notes:
1. No detection – see Sect. 4.1.
2. No detection – the field is offset from ϵ Ori by 1^m in RA.
3. No result – problems with atmospheric correction on the secondary calibrator.

would have improved the signal-to-noise ratio slightly, it broadens the beam and can result in the partial merging of the two sources visible in Fig. 1. In addition, a taper is also applied to the longest baselines (i.e. they are given less weight). We use a taper that is as large as possible but that still gives an acceptable image.

3.4. Results

The resulting fluxes are listed in Table 4 and plotted in Fig. 3, right panel. The fluxes measured for ϵ Ori are the same to within the error bars, except for the 1999 February 5 observation at 6 cm.

As a check we also measured the fluxes of some other sources present on the maps (not shown in Fig. 1), to see if there were systematic variations. The fluxes show a large spread, making it difficult to decide whether there is inherent variability in those sources or if there is some problem with the reduction. The 1999 February 5 fluxes are certainly not systematically the highest, so we cannot attribute the high ϵ Ori flux at that date to a reduction problem.

To judge the robustness of our flux determination, we repeated the reduction, with different weightings of distant visibilities, and natural weighting instead of robust uniform weighting. Most results fall within the 1-σ error bar. Only the 1999 February 8 data are less reliable, in the sense that they show a greater than 1-σ sensitivity to the exact values of the parameters.

We note that the 6 cm 1999 February 5 observation is the only discrepant one in the 11 data points we have. The error bars represent 1-σ errors, and from Gaussian statistics one expects about 30% of the points to be outside the $\pm 1\sigma$ range. We therefore conclude that the observations discussed in this section do not show variability.

4. Archive VLA observations

4.1. Reduction

We also checked whether ϵ Ori could be variable over much longer time-scales (up to many years) by looking at archive observations. A search of the VLA archive revealed the additional observations listed in Table 2. We also consulted the Australia Telescope Compact Array (ATCA) archive, but found no additional observations.

In many cases, the data have not been published, so we had to do the reduction ourselves. To avoid introducing systematic effects, we also re-reduced those data which do have published values. Table 5 gives the details of the

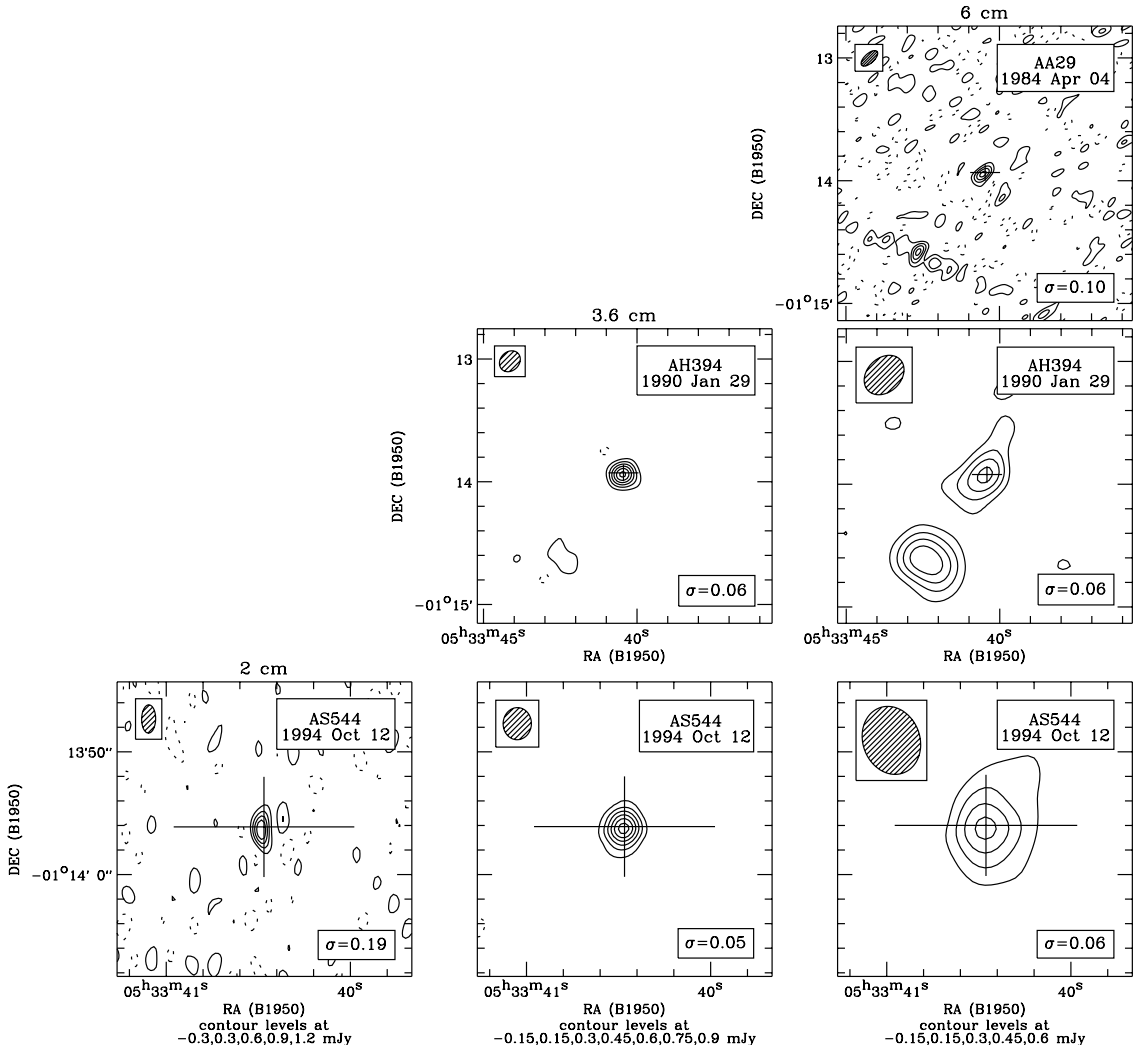

Fig. 4. Archive VLA data at 2, 3.6 and 6 cm. The bars are 1000× larger than the error bar on the Hipparcos position. Note the different spatial scale between the upper three figures and the lower three ones.

data reduction. We also added our own data to this table. The data reduction follows essentially the steps outlined in Sect. 3.2. The fluxes of the primary calibrators used are given in Table 3. The 2 cm (U-band) observations are much more sensitive to extinction in the atmosphere. They were therefore corrected for differential atmospheric extinction due to different elevations of the target and the flux calibrator (using the AIPS task ELINT).

When baseline corrections were available (for the more recent observations – from AP173 onwards), we applied them. In principle we could apply natural weighting to some of the observations because they have sufficiently high spatial resolution so that the second source will not merge with ϵ Ori. To be consistent however with the reduction of our own data, we imaged the data with robust uniform weighting (Briggs 1995). The resulting maps are shown in Figs. 2a,b and 4 and the fluxes are listed in Table 4. The 2 cm error bars include a 5% calibration error, which is somewhat higher than for 3.6 and 6 cm because of atmospheric effects.

Table 4 shows that there are only upper limits available for 20 cm (L-band) and 90 cm (P-band). There is an additional observation available (AC308 – see Table 2) made at 20 cm. This observation is part of the NRAO VLA Sky Survey (NVSS – Condon et al. 1998). We checked this survey and found that ϵ Ori was not detected.

We again checked that our measured fluxes are not very sensitive to changes in the parameters of the reduction. When we change weights for distant baselines, or used more flagging or natural weighting instead of robust uniform we find results within the error bar of the original reduction.

For some observations, we can compare our results to the published ones (Table 4 versus Table 6). The 3.6 cm fluxes are in good agreement. At 2 cm, the Scuderi et al. (1998) value of 1.40 ± 0.10 mJy is somewhat lower than our 1.65 ± 0.20 mJy. Their map was derived with natural weighting, contrary to our robust uniform weighting. When we redo our map with natural weighting we find 1.54 ± 0.17 mJy which is acceptably close to the

Table 6. Observed radio and millimetre fluxes from the literature.

λ	flux (mJy)	reference
1.2 mm	12 ± 4	Altenhoff et al. (1994)
1.3 mm	13.1 ± 2.2	Leitherer & Robert (1991)
2 cm	1.40 ± 0.10	Scuderi et al. (1998)
3.6 cm	1.04 ± 0.04	Scuderi et al. (1998)
6 cm	0.60 ± 0.06	Scuderi et al. (1998)
6 cm	1.6 ± 0.5	Abbott et al. (1980)

Scuderi et al. value. We note that our 6 cm fluxes tend to be higher than those derived by Scuderi et al. (1998) and Howarth (2000, personal communication). We suspect that our cleaning is less deep than that of others (see Sect. 3.3). Cleaning too deep can easily lower the flux by 1 σ.

The main difference between our results and published values concerns the BIEG data, on which the Abbott et al. (1980) value of 1.6 ± 0.5 mJy is based. Our re-reduction of this dataset, as well as many variant reductions (heavier flagging, less closure errors, more tapering) never resulted in a convincing detection. It should be recalled that this observation was done in 1978. At that time the VLA was not yet complete (10 antennas instead of the standard 27) and little experience was available with the reduction of this type of data. Abbott et al. also note problems with closure errors and the fact that ϵ Ori looks extended on their map. Our non-detection of ϵ Ori on this dataset is an important point, as a major motivation for the present study was the variability suggested by the difference between the Abbott et al. and the Scuderi et al. (1998) values.

4.2. Search for variability

Only at 3.6 cm and 6 cm do we have a sufficient number of observations to make a search for variability useful. All 3.6 cm observations fall within the range 0.95−0.99 mJy, which is somewhat smaller than the typical error bar on the flux determination. We thus conclude that the 3.6 cm observations do not show any variability.

In Fig. 3 we plotted the 6 cm fluxes as a function of time. Many observations give values around 0.75 mJy, but there are two exceptions which are closer to 0.5 mJy (the discrepant MERLIN flux will be discussed in Sect. 5). At first sight, this suggests significant variability.

It is remarkable however that both low values for the flux come from observations made with the highest spatial resolution (i.e. with the VLA in the A configuration). This could mean that we are resolving the stellar wind. Using a radius of 35 $R_\odot$ and a distance of 500 pc (Table 1), we find that the VLA beam of $0\farcs5$ in the A configuration (Table 5) corresponds to a diameter of 1500 R_*. From the Wright & Barlow (1975) formula, we find that the effective radius at 6 cm is about 40 R_*. While there is a substantial contribution to the flux from the material outside the effective radius, it would be quite at odds with the standard idea of a stellar wind to have any significant contribution outside a radius of 750 R_*.

Another explanation might be the existence of a ∼0.25 mJy background source sufficiently close to ϵ Ori, so that it is covered by the beam in the lower resolution configurations. We note however that no such target is detected on the high resolution maps. Furthermore, we can estimate the probability of finding a background extragalactic source close to ϵ Ori (Bridle 1994). Within the typical beamsize for our 1999 February observations, one expects only 0.008 sources with a flux larger than 0.25 mJy, so this explanation is not very likely either.

A third possible explanation is poor phase calibration, leading to flux loss (Thompson et al. 1986, pp. 428–432). Phase errors increase with baseline length, so the A configuration is the most sensitive to this effect. In addition, phase errors also increase with distance to the phase calibrator, and we note that the calibrator for these two observations is at $10\fdg8$, while the other (non-A) observations use calibrators at $4\fdg2$ or $4\fdg7$ distance.

An easy way to test this hypothesis is to check the various runs that each observation consists of. If there are large phase variations during the observation, there might be runs during which the atmosphere is more stable and therefore the phase errors smaller. Applying this test to AJ133, we find that run 4 (of the 6 runs) gives a flux of 0.77 mJy, while all the other runs are less than 0.60 mJy. This shows that AJ133 was probably affected by phase errors large enough to explain the flux discrepancy. When we try the same test for AJ248 we find that all runs give about the same flux, making this observation discrepant at the ∼2 sigma level.

The major aim of our 2000 December 21 observation was to test the various possible explanations proposed above. The results of that observation show that, independent of which of the 3 secondary calibrators we take, the flux is close to the 0.75 mJy average. This eliminates the possibility that we are resolving the stellar wind, or that there is a nearby background object. The effect of phase errors therefore remains the most probable cause of the discrepant fluxes of AJ133 and, possibly, AJ248. Based on that, we conclude that we do not detect variability in the 6 cm flux of ϵ Ori.

5. MERLIN observations

The initial aim of the MERLIN observations was to try and resolve the stellar wind of ϵ Ori in an attempt to directly detect the large-scale structure in the outer wind. Using a 6 cm flux of 1.6 mJy and an effective temperature of 28 000 K, we estimated an angular diameter corresponding to the effective radius of ∼40 milliarcsec (using the Wright & Barlow 1975 formula). This is comparable to the 40 milli-arcsec beamsize of the MERLIN instrument. In view of the lower 6 cm flux found from our own and the archive observations, the diameter will be smaller

(∼25 milliarcsec) and hence we do not expect to be able to resolve the stellar wind. The MERLIN observations are still useful however, as they could provide us with an additional four flux determinations.

Each observation consists of observing a flux calibrator (OQ208) and a long sequence of alternating between ϵ Ori and the secondary calibrator 0539−057 (B1950). In this alternation, ϵ Ori is observed for 4 min and the secondary for 1.5 min. The numbers for the 1999 January 28 observation are slightly different: 4.5 min and 1 min, respectively. On each observing run, the total integration time on ϵ Ori was about 5 hr.

The flux scale was set by comparing our flux calibrator (OQ208) to 3C286. Only the shortest baselines were used as OQ208 is resolved by MERLIN. 3C286 is resolved as well, leading to an accuracy in the absolute flux scale of a few percent. We found the flux of OQ208 to be 2.387 Jy at 6 cm.

The data were edited lightly to remove highly discrepant phase points (using MERLIN-specific software). The data were then passed through the standard MERLIN pipeline, which consists of a set of AIPS commands. The tasks HORUS, APCLN and CCMRG are used to make a map of the secondary calibrator. At the spatial resolution that MERLIN is capable of, it is quite possible that we start resolving the secondary calibrator. A second iteration of the three AIPS tasks is then made so that we are sure we have a good model for the secondary (which, in our case, turned out to be very close to a point source). Based on this, the gain amplitudes and phases can be determined (as in Sect. 3.2).

We then plot the gain phases and amplitudes as a function of time, and flag those time ranges that show large jumps of these quantities. As usual, phases are much more sensitive than amplitudes, so flagging is based mostly – but not exclusively – on them. The data that were not flagged then go through the pipeline a second time. At the end the ϵ Ori data are calibrated and mapped using IMAGR.

Although we tried various levels of flagging, tapering and changing other parameters, we never convincingly detected ϵ Ori on any of the observations. The RMS values of the maps are about 0.20 mJy, which means that we are probably just on the 3-sigma limit of detection.

We next combined all four calibrated observations into a single dataset and made an image (see Fig. 2c). This time we detected a source at the correct position of 0.51 ± 0.11 mJy (the error bar includes a 5% calibration error). The source is not well-fitted by a point source however. In view of the lesser quality of these data, we do not consider the source to be resolved. For the same reason, we also judge that the MERLIN result is in agreement with the VLA data, so again we find no evidence for variability.

6. JCMT observation

We observed ϵ Ori also with the Submillimetre Common-User Bolometer Array (SCUBA, Holland et al. 1999) instrument of the James Clerk Maxwell Telescope (JCMT) on Mauna Kea, Hawaii. The instrument observes simultaneously at 450 and 850 μm using two hexagonal arrays of bolometers (91 at 450 μm and 37 at 850 μm). Because of the lower sensitivity of the instrument at 450 μm, the source was only detected at 850 μm. Our flexibly scheduled observations were taken in medium weather conditions (850 μm zenith opacity was 0.36−0.48) during a half-shift on 2000 October 12. The beam at 850 μm is $14\farcs5$.

We used SCUBA in its photometry mode, where the target falls on the central pixel of the bolometer array. Chopping over $60''$ with a frequency of 7.8125 Hz was used to correct for the rapidly varying atmospheric conditions. In addition, the telescope is jiggled in a 3×3 square pattern with $2''$ steps, spending 1 s per point. This compensates for seeing and pointing irregularities. Finally, every 9 s the telescope is nodded (interchange of signal and background positions). A single integration therefore takes 18 s and 6×50 integrations were taken on the target, resulting in an on-target integration of 45 min.

To determine the transparency of the atmosphere, we measured the sky emission at various elevations (skydip) before, after, and once during the ϵ Ori observation. Pointing was regularly checked during the observation.

The reduction was done using the SCUBA User Reduction Facility (SURF, Jenness & Lightfoot 1998), version 1.5–1. Data were flatfielded and extinction corrected. The inner ring of 6 bolometers around the central pixel was used to correct the data from the central pixel for sky noise. This only works when no extended emission is present around the star, which was checked by Leitherer & Robert (1991). Using a ring also has the advantage of being less sensitive to the field rotation due to the instrument being in the Nasmyth focus. Data are averaged over the jiggle pattern resulting in the stellar flux in instrumental units. The RMS on the ϵ Ori observation is about 10%. We tried variants in the reduction (e.g. using other bolometers than the inner ring for sky-noise removal), but this gives errors less than 10%, so we do not consider them significant.

Calibration was done using HL Tau, which was observed in photometry mode in the middle of the ϵ Ori runs. The calibration does introduce significant additional uncertainty. Formally we arrive at 21.6 ± 2.6 mJy for the flux. This takes into account the measurement errors on the target and the calibrator as well as the calibration error. However if we use the HL Tau calibration observation that follows our run, instead of the one in the middle, we have 17.3 ± 2.1 mJy. Trying to use other calibrators that were observed during that night (but of course further away in time from our observation) tends to favour the lower value. In view of this we propose the lower value as the best determination of the flux. As can be seen from Table 6, this value is in very good agreement with the 1.3 mm determination of Leitherer & Robert (1991) and the 1.2 mm observation of Altenhoff et al. (1994).

Table 7. Mass loss rate determinations from the literature.

wavelength	$\log \dot{M}(M_\odot/\mathrm{yr})$	reference
radio	-5.51 ± 0.2	Abbott et al. (1980)
	-5.39 ± 0.16	Lamers & Leitherer (1993)
	-5.68 ± 0.06	Scuderi et al. (1998)
IR+radio	-5.48	Lamers & Waters (1984)
Hα	-5.80	Olson & Ebbets (1981)
	-5.76	Leitherer (1988)
	-5.59 ± 0.18	Lamers & Leitherer (1993)
	-5.48	Puls et al. (1996)
	-5.62	Kudritzki et al. (1999)

7. Discussion

7.1. Fluxes and variability

We list the fluxes that will be fitted. For the 850 μm observation, we simply use the result from Sect. 6, i.e. 17.3 ± 2.1 mJy. As we found no variability for the radio observations, we average the fluxes to determine the best values. We find 0.96 ± 0.08 mJy at 3.6 cm and 0.74 ± 0.13 mJy at 6 cm. The 6 cm average does not include the AJ133 and MERLIN observations, for reasons explained in Sects. 4.2 and 5 respectively. The standard deviation was calculated by adding (in RMS sense) the average of the standard deviations on the fluxes and the standard deviation on the averages. Using a 3-sigma criterion, this puts an upper limit of $\pm 25\%$ on the variability of the 3.6 cm flux. In principle, this could be used to set limits on the strength of the large-scale structure in the radio formation region. For the present dataset, however, the constraints are bound to be extremely weak, so we did not attempt any detailed modelling.

7.2. Smooth wind model

The model we apply is the same one as Runacres & Blomme (1996 – hereafter RB96) used to study the long-wavelength continuum radiation of a number of early-type stars, including ϵ Ori. They calculated the continuum flux by solving the equations of radiative transfer and statistical equilibrium in a spherically symmetric model for the stellar wind. The density was determined by solving the time-independent hydrodynamics, following Pauldrach et al. (1986). When fitting the model to the observations, the visual and near-infrared fluxes were used to determine the interstellar extinction and the radio fluxes to determine the mass-loss rate. The far-infrared and millimetre fluxes are unconstrained and can therefore be used to see how well the smooth wind model fits the observations. For further details we refer to RB96.

We redid their calculation for ϵ Ori, taking into account the revised 6 cm flux as well as the newly determined 850 μm and 3.6 cm fluxes. We also took the opportunity to change the stellar parameters to be in agreement with those of Kudritzki et al. (1999): $T_{\mathrm{eff}} = 28\,500$ K, $\log g(\mathrm{cgs}) = 3.00$; $Y = 0.1$; $v_\infty = 1\,600$ km s^{-1}, $D = 500$ pc.

We made the best fit go through the 3.6 cm radio observation, as this wavelength has a number of flux determinations, none of which is discrepant. The best fit gives a mass-loss rate of $\log \dot{M} = -5.73 \pm 0.04$ ($\dot{M}$ in $M_\odot$/yr). The error bar on $\log \dot{M}$ was derived from the error bar on the 3.6 cm flux, and using $\dot{M} \propto \mathrm{flux}^{0.75}$ (Wright & Barlow 1975). To get a more realistic error estimate, we note that one of the more important uncertainties is the Hipparcos distance, which translates into a $(-0.30, +0.16)$ error bar on $\log \dot{M}$. If we would have used the 6 cm flux, we would have arrived at a mass loss rate of $\log \dot{M} = -5.71 \pm 0.07$.

Our mass-loss rate is of course significantly lower than previous mass-loss rates based on the Abbott et al. (1980) observation at 6 cm (see Table 7). Our value is in good agreement with the Scuderi et al. (1998) value, which is based on a much lower flux at 6 cm. The agreement with the wind momentum-luminosity relation is also very good. The modified wind momentum $(\dot{M} v_\infty (R_*/R_\odot)^{0.5})$ differs from the Kudritzki et al. (1999) best fit relation to $\log L/L_\odot$ by only 0.1 dex.

It is interesting to note the acceptable agreement (0.1 dex) with the Hα mass-loss determination of Kudritzki et al. (1999). In view of the fact that we calculated our model with exactly the same parameters (except the mass-loss rate), these results are directly comparable. The known variability in the Hα profile (e.g. Ebbets 1982) can be translated into an approximately ± 0.1 dex variation on the mass-loss rate, using Fig. 15 of Puls et al. (1996). The good agreement between Hα and radio mass-loss rates for early-type stars in general has been pointed out by Lamers & Leitherer (1993). One possible interpretation is that there is no significant structure in either formation region (as Lamers & Leitherer conclude). The other possibility is that the structure is the same near the stellar surface and at large distance, but in that case it remains puzzling why the amount of structure should be so closely the same in these very different formation regions.

The best fit result is shown in Fig. 5. The visual and infrared observational data were collected from the literature by RB96. We eliminated a highly discrepant 18 μm observation because of the possibility of a blue leak in the filter used (Barlow & Cohen 1977). In contrast to what RB96 found for ϵ Ori, there now is a clear excess in the millimetre region. The excess is larger (67%) than what they had found for ζ Pup (35%), and is significant at the 3-sigma level. Furthermore, the IRAS 25 μm infrared flux is also significantly larger (2.9 sigma) than what a smooth wind predicts. This means that ϵ Ori now joins the group of four other stars (α Cam, δ Ori A, κ Ori and ζ Pup) for which RB96 found significant infrared and/or millimetre excess. While it has been claimed that the infrared excesses can be explained by a slower velocity law (Kudritzki & Puls 2000), a different velocity law will have little effect on the millimetre excess.

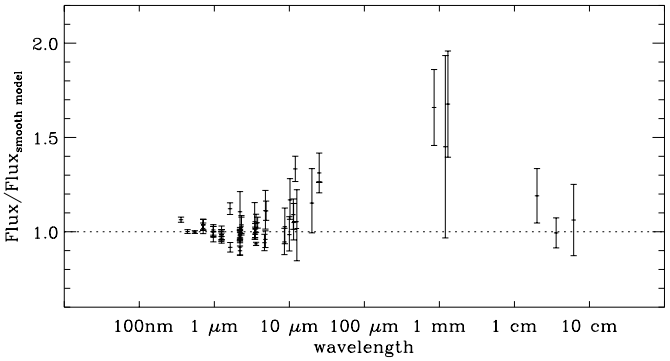

Fig. 5. Observed fluxes normalised to a smooth wind model. Observations above the dotted line point to additional emission that is not included in the smooth model.

7.3. Modelling the millimetre excess

The excess in the millimetre region points to an additional emission mechanism that is not included in the model of Sect. 7.2. Due to the properties of the millimetre and radio emission (bremsstrahlung), a structured wind emits more than a smooth wind with the same mass-loss rate (Sect. 1). We repeat that there is a wealth of evidence that the winds of early-type stars are indeed highly structured. We therefore suggest that the most plausible explanation for the excess is structure in the millimetre formation region, either small-scale or large-scale. Without claiming that large-scale structure can be excluded, we favour small-scale structure in view of the detail of the theoretical models, and the fact that its effect on the long-wavelength continuum can be described by a single parameter, namely the clumping factor (see Runacres & Owocki 2001).

The clumping factor is defined as $< \rho^2 > / < \rho >^2$, where the symbol $<>$ stands for a time-average, which we have approximated by integrating over a small volume of the wind. In the simplifying assumption that essentially all material is concentrated in clumps, with negligible inter-clump mass, the clumping factor is the inverse of the volume filling factor.

We introduced the clumping factor into a Wright & Barlow (1975) type model. The opacity calculated in the smooth wind is multiplied by the clumping factor to get the clumped wind opacity. We also extended the Wright & Barlow model to include a velocity law instead of using a constant velocity. For the velocity law, we take $v(r)/v_\infty = 0.01 + 0.99(1 - R_*/r)^\beta$, with $\beta = 1$. The calculation of the flux then proceeds as in Wright & Barlow. As our model allows the clumping factor and velocity to change as a function of distance, all integrations have to be done numerically.

We used a run of the clumping factor based on the work of Runacres & Owocki (2001). They calculated time-dependent hydrodynamical models, to study the effect of the line-driving instability at large distances from the star. The clumping factor in their models rises to reach a maximum rather far away from the star (10−50 R_*) and then decreases again. If we simplify their results somewhat, we

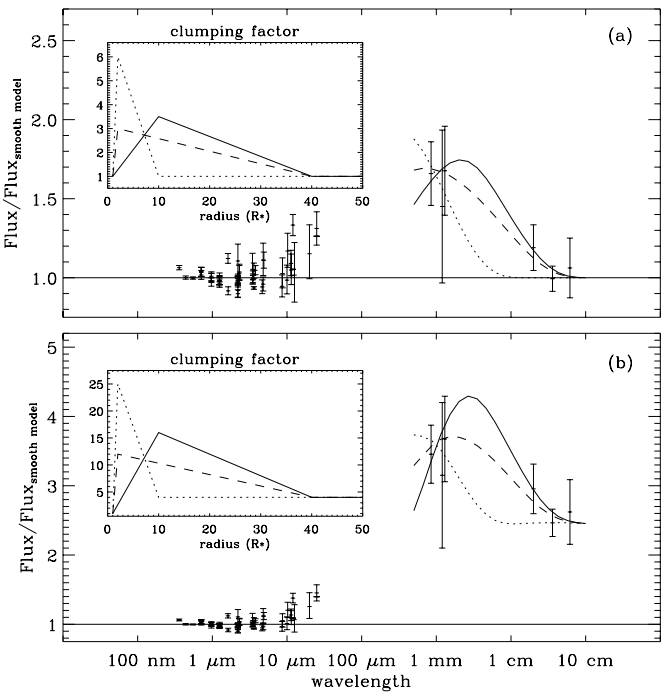

Fig. 6. The millimetre excess is fitted with a structured wind model. Three possible runs of the clumping factor as a function of radius are used (inset). **a)** Assumes that no structure is present in the radio formation region (i.e. no structure beyond 40 R_*, which is the Wright & Barlow (1975) effective radius for 6 cm emission), while **b)** does have structure in the radio formation region.

can describe a typical behaviour for the clumping factor as follows: it starts at 1.0 just above the stellar surface, increases up to a large distance and then declines further out.

In a first series of experiments, we assumed that there is *no* structure in the radio formation region. This assumption is consistent with the fitting procedure used in Sect. 7.2. We tried various runs of the clumping factor as a function of distance. To keep the model simple we use a piece-wise linear curve: we let the clumping factor rise linearly from the surface of the star to a certain distance, and then let it fall off again linearly (see inset Fig. 6a). By setting the clumping factor equal to one beyond 40 R_*, we ensure that there is no excess at radio wavelengths. As the present model is too simple to allow the accurate calculation of infrared fluxes, we limited ourselves to millimetre and radio fluxes. Figure 6a shows that various runs of the clumping factor can result in a model that fits the observed millimetre fluxes. One can see that the geometric extent of the structure is still not well constrained with the wavelength coverage available at the moment. A clumping factor with a value of 3−6 can explain the observed millimetre excess.

A second series of experiments does include structure in the radio formation region. This is more consistent with the Runacres & Owocki (2001) results which show the clumping factor reaches a value of ∼4 at the outer limit

of their grid (100 R_*). Again we modelled this behaviour using a piece-wise linear curve. Because of the structure in the radio formation region we need to decrease the mass-loss rate by a factor of two to be able to fit the observed radio fluxes. The results (Fig. 6b) are similar to the results from our first series of models, except that the clumping factors are considerably larger (10−25).

Finally one might try to explain the observations by the effect of recombination at distances larger than $\sim$10 R_*. We note that even in our standard model (Sect. 7.2) all He has already recombined to He^+ above a few stellar radii. Again we can use a Wright & Barlow type model in which piece-wise linear curves for the ionization fraction of H and He are tried. It turns out to be impossible to explain the observations without at least a partial recombination of hydrogen starting at $\sim$10 R_*. It seems very unlikely that this can be the case at such a small distance from the surface of a star with an effective temperature of 28 500 K.

8. Conclusions

We studied the stellar wind of ϵ Ori at submillimetre and radio wavelengths, supplementing our own observations with archive data. Based on the derived fluxes and on our failure to detect ϵ Ori on the re-reduced data of Abbott et al. (1980), we believe their 1.6 ± 0.5 mJy determination at 6 cm to be in error.

We determine a flux of 0.96 ± 0.08 mJy at 3.6 cm and 0.74 ± 0.13 mJy at 6 cm. The dataset does not indicate any variability at more than the $\pm$25% level. The resulting mass-loss rate, $\log \dot{M}(M_\odot/\mathrm{yr}) = -5.73 \pm 0.04$, is in good agreement with the Hα determination by Kudritzki et al. (1999).

We also modelled the newly determined fluxes and found a significant excess of radiation in the millimetre region, indicating increased structure in the inner $\sim$10 R_*. It is clear from Fig. 6 that an additional observation at 7 mm could severely constrain the amount of structure as a function of distance in the *millimetre* formation region. To decide on the existence of structure in the *centimetre* region, observations at 20 cm are needed.

The lack of radio variability suggests that structure in the radio formation region, if it exists, is more of a stochastic nature, rather than in the form of CIRs. However, the present data still do not provide strong constraints on this. A critical test on the extent of large-scale structure is to search for variability at far-infrared to millimetre wavelengths.

Acknowledgements. We very much appreciate the help given by the VLA data analysts in preparing our observations and in transferring archive data. We are grateful to Jim Condon (NRAO, Charlottesville) for his help with the reduction of the VLA data. The reduction of the MERLIN data was done with the help of Simon Garrington. We thank Thomas Lowe for making the JCMT observation. This work also profited from discussions with J. Bieging, S. Clark, C. Stanghellini and G. van de Steene. We also want to thank Sarah Kendrew for her help in the data reduction. This research has made use of the SIMBAD database, operated at CDS, Strasbourg, France and NASA's Astrophysics Data System Abstract Service. M.C.R. acknowledges support from ESA-Prodex project no. 13346/98/NL/VJ(ic). S.C. is grateful for the support of PPARC.

References

Abbott, D. C., Bieging, J. H., Churchwell, E., & Cassinelli, J. P. 1980, ApJ, 238, 196
Altenhoff, W. J., Thum, C., & Wendker, H. J. 1994, A&A, 281, 161
Baars, J. W. M., Genzel, R., Pauliny-Toth, I. I. K., & Witzel, A. 1977, A&A, 61, 99
Barlow, M. J., & Cohen, M. 1977, ApJ, 213, 737
Berghöfer, T. W., Schmitt, J. H. M. M., & Cassinelli, J. P. 1996, A&AS, 118, 481
Bridle A. H. 1994, in ASP Conf. Ser. 6, Synthesis Imaging in Radio Astronomy, ed. R. A. Perley, F. R. Schwab, & A. H. Bridle, 443
Briggs, D. S. 1995, High Fidelity Deconvolution of Moderately Resolved Sources, Ph.D. Thesis (The New Mexico Institute of Mining and Technology, Socorro, New Mexico)
Cassinelli, J. P., & Swank, J. H. 1983, ApJ, 271, 681
Cassinelli, J. P., Myers, R. V., Hartmann, L., Dupree, A. K., & Sanders, W. T. 1983, ApJ, 268, 205
Chen, W., & White, R. L. 1991, ApJ, 366, 512
Collura, A., Sciortino, S., Serio, S., et al. 1989, ApJ, 338, 296
Condon, J. J. 1997, PASP, 109, 166
Condon, J. J., Cotton, W. D., Greisen, E. W., et al. 1998, AJ, 115, 1693
Cornwell, T., & Braun, R. 1994, in Synthesis Imaging in Radio Astronomy, ed. R. A. Perley, F. R. Schwab, & A. H. Bridle, ASP Conf. Ser., 6, 167
Cranmer, S. R., & Owocki, S. P. 1996, ApJ, 462, 469
Dougherty, S. M., & Taylor, A. R. 1992, Nature, 359, 808
Ebbets, D. 1982, ApJS, 48, 399
ESA 1997, The Hipparcos and Tycho Catalogues, ESA SP-1200
Groenewegen, M. A. T., & Lamers, H. J. G. L. M. 1989, A&AS, 79, 359
Hanbury Brown, R., Davis, J., & Allen, L. R. 1974, MNRAS, 167, 121
Holland, W. S., Robson, E. I., Gear, W. K., et al. 1999, MNRAS, 303, 659
Humphreys, R. M. 1978, ApJS, 38, 309
Jenness, T., & Lightfoot, J. F. 1998, in Astronomical Data Analysis Software and Systems VII, ed. R. Albrecht, R. N. Hook, & H. A. Bushouse, ASP Conf. Ser., 145, 216
Johnson, H. L., & Morgan, W. W. 1953, ApJ, 117, 313
Kaufer, et al. 2001, in preparation
Kudritzki, R. P., & Puls, J. 2000, ARA&A, 38, 613
Kudritzki, R. P., Gabler, A., Gabler, R., Groth, H. G., & Pauldrach, A. W. A. 1989, in Physics of Luminous Blue Variables, ed. K. Davidson, A. F. J. Moffat, & H. J. G. L. M. Lamers (Kluwer, Dordrecht), IAU Colloq., 113, 67
Kudritzki, R. P., Puls, J., Lennon, D. J., et al. 1999, A&A, 350, 970
Lamers, H. J. G. L. M., & Leitherer, C. 1993, ApJ, 412, 771
Lamers, H. J. G. L. M., & Waters, L. B. F. M. 1984, A&A, 136, 37

Leitherer, C. 1988, ApJ, 326, 356
Leitherer, C., & Robert, C. 1991, ApJ, 377, 629
Levato, H., Morrell, N., Garcia, B., & Malaroda, S. 1988, ApJS, 68, 319
Lucy, L. B. 1982, ApJ, 255, 278
Lupie, O. L., & Nordsieck, K. H. 1987, AJ, 93, 214
McErlean, N. D., Lennon, D. J., & Dufton, P. L. 1998, A&A, 329, 613
McErlean, N. D., Lennon, D. J., & Dufton, P. L. 1999, A&A, 349, 553
Mermilliod, J.-C. 1987, A&AS, 71, 413
Mullan, D. J. 1986, A&A, 165, 157
Olson, G. L., & Ebbets, D. 1981, ApJ, 248, 1021
Owocki, S. P. 1999, in Variable and Non-spherical Stellar Winds in Luminous Hot Stars, ed. B. Wolf, O. Stahl, & A.W. Fullerton, Lecture Notes in Physics (Springer, Berlin), 294
Owocki, S. P. 2000, Radiatively Driven Stellar Winds from Hot Stars, in Encyclopedia of Astronomy and Astrophysics, http://www.ency-astro.com (London: Nature Publishing Group, and Bristol: Institute of Physics Publishing)
Pallavicini, R., Golub, L., Rosner, R., et al. 1981, ApJ, 248, 279
Pauldrach, A., Puls, J., & Kudritzki, R. P. 1986, A&A, 164, 86
Perley, R. A., & Taylor, G. B. 1999, The VLA Calibrator Manual (http://www.aoc.nrao.edu/∼gtaylor/calib.html)
Prinja, R. K. 1998, in Cyclical Variability in Stellar Winds, ed. L. Kaper, & A. W. Fullerton, ESO Astroph. Symp. (Springer, Berlin), 92
Prinja, R. K., & Howarth, I. D. 1986, ApJS, 61, 357
Prinja, R. K., Barlow, M. J., & Howarth, I. D. 1990, ApJ, 361, 607
Prinja, R. K., Massa, D., & Fullerton, A. W. 2001, in preparation
Puls, J., Kudritzki, R. P., Herrero, A., et al. 1996, A&A, 305, 171
Runacres, M. C., & Blomme, R. 1996, A&A, 309, 544 (RB96)
Runacres, M. C., & Owocki, S. P. 2001, A&A, submitted
Sciortino, S., Vaiana, G. S., Harnden Jr., F. R., et al. 1990, ApJ, 361, 621
Scuderi, S. 1994, Ph.D. Thesis, University of Catania
Scuderi, S., Panagia, N., Stanghellini, C., Trigilio, C., & Umana, G. 1998, A&A, 332, 251
Skinner, C. J., Exter, K. M., Barlow, M. J., Davis, R. J., & Bode, M. F. 1997, MNRAS, 288, L7
Snow Jr., T. P., York, D. G., & Welty, D. E. 1977, AJ, 82, 113
Thompson, A. R., Moran, J. M., & Swenson Jr., G. W. 1986, Interferometry and Synthesis in Radio Astronomy (Wiley-Interscience, New York)
White, R. L., & Becker, R. H. 1982, ApJ, 262, 657
Williams, P. M., Dougherty, S. M., Davis, R. J., et al. 1997, MNRAS, 289, 10
Wright, A. E., & Barlow, M. J. 1975, MNRAS, 170, 41